Electronic Supplementary Material (ESI) for Environmental Science: Nano.

Supporting Information

Hierarchical Z-Scheme g-C_3N_4/Au/$ZnIn_2S_4$ Photocatalyst for Highly Enhanced Visible-Light Photocatalytic Nitric Oxide Removal and Carbon Dioxide Conversion

Guping Zhang,[a] Xingwang Zhu,[b] Dongyun Chen,*[,a] Najun Li,[a] Qingfeng Xu,[a] Hua Li,[a] Jinghui He,[a] Hui Xu,[b] and Jianmei Lu*[,a]

[a]College of Chemistry, Chemical Engineering and Materials Science, Collaborative Innovation Center of Suzhou Nano Science and Technology Soochow University, Suzhou 215123 (P.R. China)

[b]Institute for Energy Research, Jiangsu University, Zhenjiang 212013 (P.R. China)

E-mail: dychen@suda.edu.cn; lujm@suda.edu.cn

Table of Contents

S1. SEM images of as-prepared samples

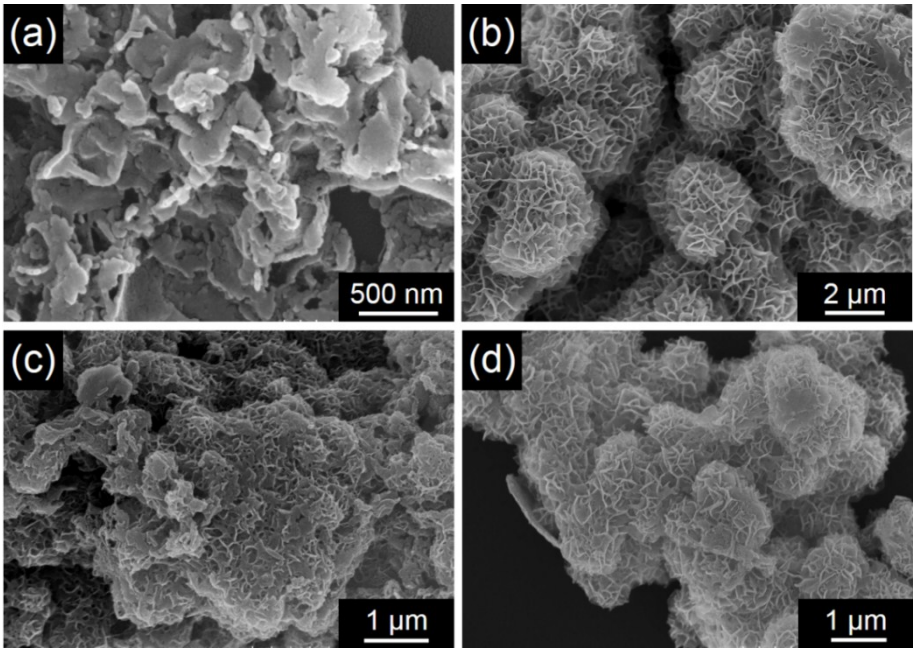

Figure S1. SEM images of as-prepared (a) CN, (b) $ZnIn_2S_4$, (c) CN/Au/ZIS-0.5 and (d) CN/Au/ZIS-2.

S2. TEM-EDX of as-prepared samples

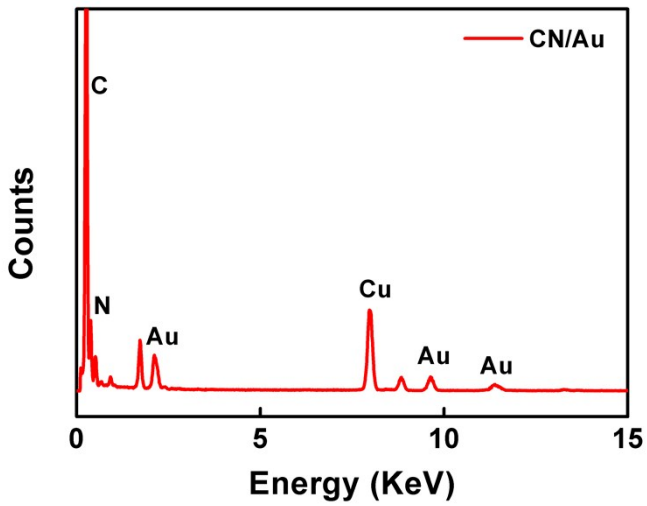

Figure S2. TEM-EDX of as-prepared CN/Au.

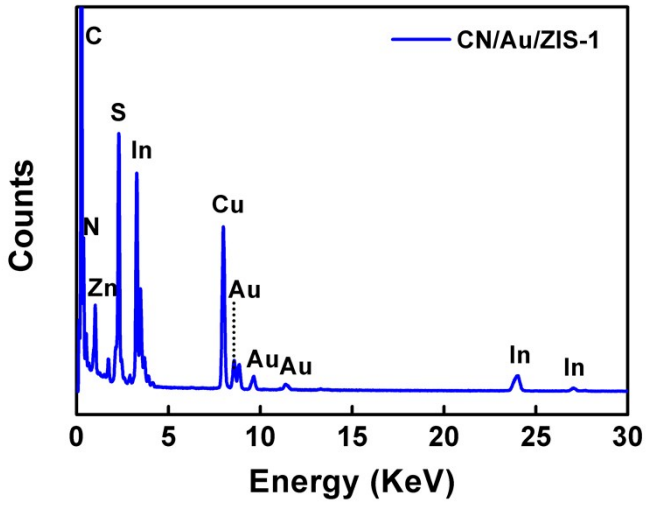

Figure S3. TEM-EDX of as-prepared CN/Au/ZIS-1.

S3. Survey XPS spectrum of CN/Au/ZIS-1 sample

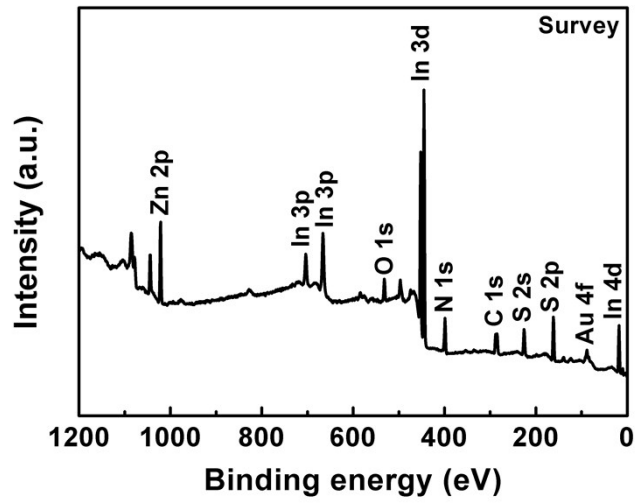

Figure S4. Survey XPS spectrum of the CN/Au/ZIS-1 sample.

S4. Valence-band XPS of CN and $ZnIn_2S_4$ samples

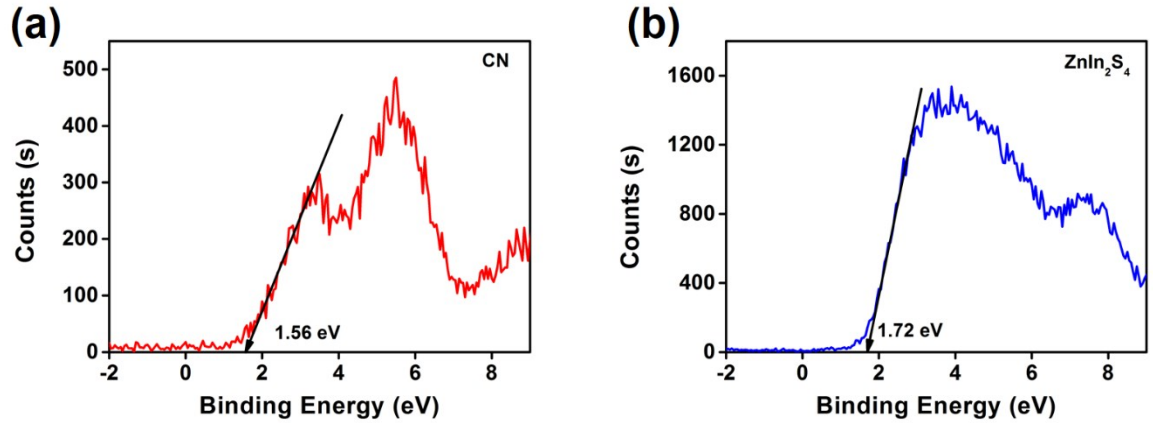

Figure S5. Valence-band XPS spectra of CN and $ZnIn_2S_4$ samples.

S5. Pore size distribution curve of CN/Au/ZIS-1 sample

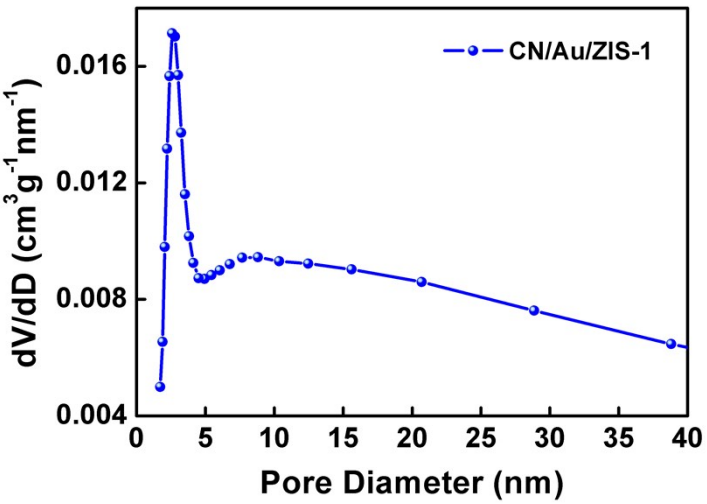

Figure S6. Pore size distribution curves of obtained CN/Au/ZIS-1 sample.

S6. EIS and time-resolved transient PL spectra of as-prepared samples

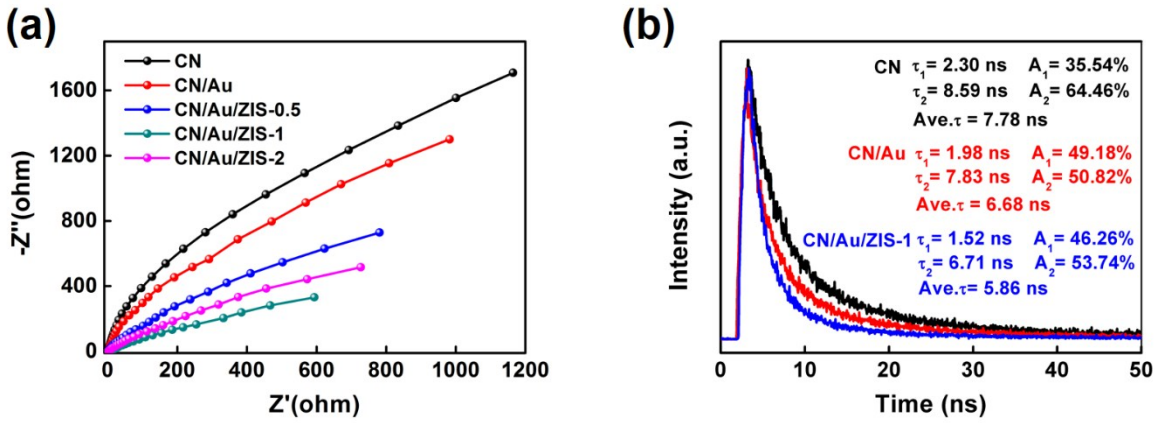

Figure S7. EIS spectra (a) and time-resolved transient PL decay (b) of the as-prepared samples.

S7. Photocatalytic activities of prepared samples and Detecting of NO_2

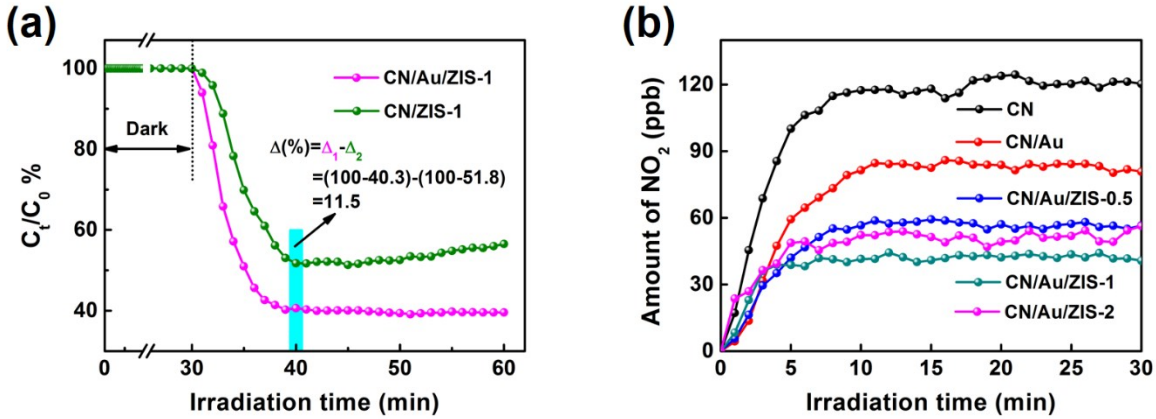

Figure S8. (a) Visible-light photocatalytic activities of the CN/Au/ZIS-1 and CN/ZIS-1 samples for NO removal in air (600 ppb). (b) Monitoring of NO_2 intermediates during irradiation.

S8. Detecting of H_2O_2 and ·OH

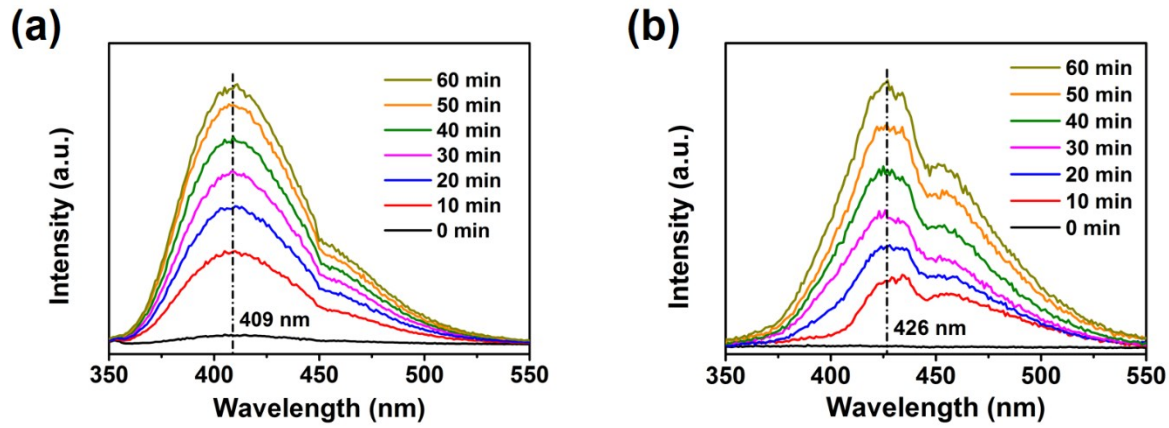

Figure S9. The fluorescence intensity of (a) H_2O_2 and (b) ·OH-trapping PL spectra of the CN/Au/ZIS-1 at different visible light irradiation times.

S9. Photocatalytic CO_2 conversion without 2,2-bipyridine (bpy)

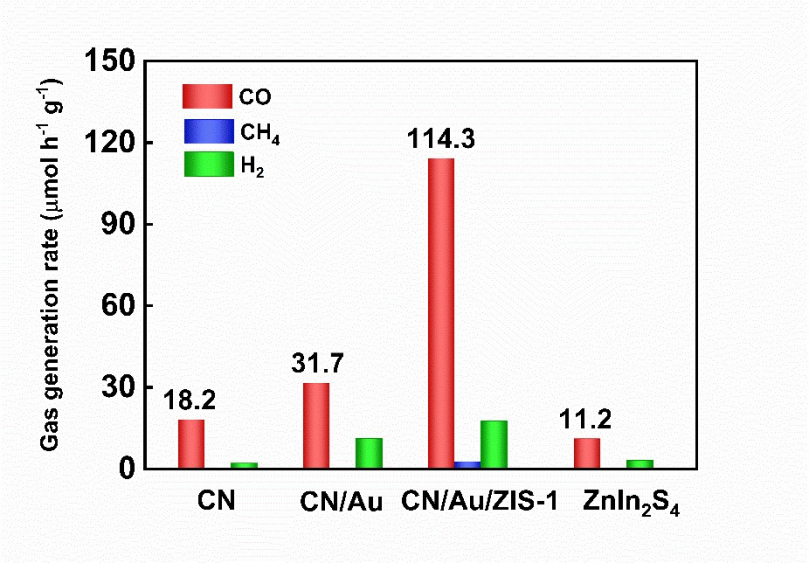

Figure S10. CO_2 photoreduction activities of different samples without 2,2-bipyridine (bpy).

S10. The calculation about the N-balance

The concentration of NO_3^- detected by ion chromatography, the washing solution (1000 mL) was concentrated 100 times before the detection. Therefore, the concentration of NO_3^- in washing solution should be 0.016 mg/L.

(1) The consumption of NO (C_{NO}): $C_{NO} = \sum_{t=1}^{t=30} NOc$ = 8746 ppb =8.746 ppm.

The concentration of consumption NO (C_{NO}) is: $C_{NO} = \frac{30 \times 8.746}{22.4}$ = 11.713 μg/L;

(2) The generated NO_2 (C_{NO2}) is: $C_{NO2} = \sum_{t=1}^{t=30} NO_2c$ = 3153 ppb = 3.153 ppm.

The concentration of NO which converted to NO_2 ($C_{NO/NO2}$) is： $C_{NO/NO2} = \frac{30 \times 3.153}{22.4}$ = 4.223 μg/L;

(3) The concentration NO which converted to HNO_3 ($C_{NO/HNO3}$) is:

$C_{NO/NO3-} = \frac{0.016}{62} \times 30$ = 0.007742 mg/L = 7.742 μg/L;

(4) $C_{NO/NO3-} + C_{NO/NO2}$ = 7.742 + 4.223 = 11.965μg/L; this value approximately equal to that of consumption NO, therefore, the formed NO_2, and NO_3^- can meet with the consumed NO.

S11. Table S1 Data comparison of photocatalytic NO removal over different catalysts.

Catalyst	Catalyst (mg)	NO (ppb)	Light type (Xe lamp)	Time (min)	$\eta_{(NO)}$ (%)	Ref
$Bi_2Sn_2O_7$	200	400	300 W	60	37.0	[1]
CQDs-FeOOH	100	400	300 W	30	34.0	[2]
BiOBr-graphene	100	400	300 W	30	40.0	[3]
$Bi_2O_2CO_3$-g-C_3N_4	100	400	300 W	30	34.8	[4]
Bi@BiOSi	200	450	150 W	30	50.2	[5]
CN-OLa	100	500	150 W	30	50.4	[6]
$LaFeO_3$-$SrTiO_3$	100	400	300 W	30	40.0	[7]
g-C_3N_4/$LaCO_3OH$	100	400	300 W	30	30.3	[8]
$SrFe_xTi1_{-x}O_{3-\delta}$	100	400	300 W	30	35.0	[9]
OV-$Bi_2O_2CO_3$	200	600	150 W	30	50.2	[10]
BiOCl/PPy	100	600	300 W	30	28.0	[11]
BiOBr-3C	200	600	150 W	30	38.7	[12]
PI-g-C_3N_4	50	600	300 W	50	47.0	[13]
Au@CN	200	500	150 W	30	41.0	[14]
N-TiO_2/g-C_3N_4	200	600	300 W	30	46.1	[15]

N-doped TiO_2	100	600	150 W	30	36.5	[16]
g-C_3N_4/Au/$ZnIn_2S_4$	**100**	**600**	**300 W**	**30**	**59.7**	**This work**

S12. Table S2 Data comparison of photocatalytic CO_2 reduction over different catalysts.

Catalyst	Experimental system	Light type (Xe lamp)	Products (μmol h^{-1} g^{-1})	Ref
In_2S_3-$CuInS_2$	$CoCl_2$, 2,2-bipyridine, TEOA, MeCN	300 W	CO: 19	[17]
g-C_3N_4	$CoCl_2$, 2,2-bipyridine, TEOA, MeCN	300 W	CO: 6	[18]
BCN	$CoCl_2$, 2,2-bipyridine, TEOA, MeCN	300 W	CO: 94	[19]
Nitrogen-rich g-C_3N_4 nanotubes	$CoCl_2$, 2,2-bipyridine, TEOA, MeCN	300 W	CO: 103.6	[20]
UiO-66/CNNS	TEOA, MeCN	300W	CO: 9.79	[21]
N-Ta_2O_5	$[Ru(dcbpy)_2(CO)_2]^{2+}$ TEOA	300 W	HCOOH: 70	[22]
RuRu'/NS-C_3N_4	Ag, EDTA·2Na	300 W	$HCOO^-$: 57.5	[23]
Helical g-C_3N_4	$CoCl_2$, TEOA and MeCN	300 W	CO: 89	[24]
CeO_2 homojunction	0.5 wt %Pt/0.5 wt % MnO_x, CO_2 and H_2O	300 W	CH_4: 0.086	[25]
GaN nanowires array	0.5 wt %Pt, CO_2 and H_2O vapor	300 W	CH_4: 14.8	[26]

$Cu_3(BTC)_2$@TiO_2	CO_2 and H_2O vapor	300 W	CH_4: 2.6	[27]
$CaTaO_2N$	1.0 wt % Ag, CH_3OH, CO_2 bubbled	500 W	CO: 0.35	[28]
g-C_3N_4/Au/$ZnIn_2S_4$	**$CoCl_2$, 2,2-bipyridine, TEOA, MeCN**	**300 W**	**CO: 242.3**	**This work**

S13. Reference

[1] Y. Lu, Y. Huang, J. Cao, W. Ho, Q. Zhang, D. Zhu, S. Lee, Insight into the Photocatalytic Removal of NO in Air over Nanocrystalline $Bi_2Sn_2O_7$ under Simulated Solar Light, *Ind. Eng. Chem. Res.* 2016, **55**, 10609-10617.

[2] Y. Huang, Y. Gao, Q. Zhang, Y. Zhang, J. Cao, W. Ho, S. Lee, Biocompatible FeOOH-Carbon quantum dots nanocomposites for gaseous NO_x removal under visible light: Improved charge separation and High selectivity, *J. Hazard. Mater.* 2018, **354**, 54-62.

[3] Z. Ai, W. Ho, S. Lee, Efficient visible light photocatalytic removal of NO with BiOBr-graphene nanocomposites, *J. Phys. Chem. C* 2011, **115**, 25330-25337.

[4] Z. Wang, Y. Huang, W. Ho, J. Cao, Z. Shen, S. Lee, Fabrication of $Bi_2O_2CO_3$/g-C_3N_4 heterojunctions for efficiently photocatalytic NO in air removal: In-situ self-sacrificial synthesis, characterizations and mechanistic study, *Appl. Catal., B* 2016, **199**, 123-133.

[5] X. Li, W. Zhang, J. Li, G. Jiang, Y. Zhou, S. Lee, F. Dong, Transformation pathway and toxic intermediates inhibition of photocatalytic NO removal on designed Bi metal@defective $Bi_2O_2SiO_3$, *Appl. Catal., B* 2019, **241**, 187-195.

[6] P. Chen, H. Wang, H. Liu, Z. Ni, J. Li, Y. Zhou, F. Dong, Directional electron delivery and enhanced reactants activation enable efficient photocatalytic air purification on amorphous carbon nitride co-functionalized with O/La, *Appl. Catal., B* 2019, **242**, 19-30.

[7] Q. Zhang, Y. Huang, S. Peng, Y. Zhang, Z. Shen, J. Cao, W. Ho, S. Lee, D. Pui, Perovskite $LaFeO_3$-$SrTiO_3$ composite for synergistically enhanced NO removal under visible light excitation, *Appl. Catal., B* 2017, **204**, 346-357.

[8] Z. Wang, H. Yu, C. Long, M. Chen, J. Cao, W. Ho, S. Lee, In situ g-C_3N_4 self-sacrificial synthesis of a g-C_3N_4/$LaCO_3OH$ heterostructure with strong interfacial charge transfer and separation for photocatalytic NO removal, *J. Mater. Chem. A* 2018, **6**, 972-981.

[9] Q. Zhang, Y. Huang, S. Peng, T. Huang, J. Cao, W. Ho, S. Lee, Synthesis of $SrFe_xTi_{1-x}O_{3-\delta}$ nanocubes with tunable oxygen vacancies for selective and efficient photocatalytic NO oxidation, *Appl. Catal. B* 2018, **239**, 1-9.

[10] H. Liu, P. Chen, X. Yuan, Y. Zhang, H. Huang, L. Wang, F. Dong, Pivotal roles of artificial oxygen vacancies in enhancing photocatalytic activity and selectivity on $Bi_2O_2CO_3$ nanosheets, *Chinese J. Catal.* 2019, **40**, 620-630.

[11] Z. Zhao, Y. Cao, F. Dong, F. Wu, B. Li, Q. Zhang, Y. Zhou, The activation of oxygen through oxygen vacancies in BiOCl/PPy to inhibit toxic intermediates and enhance the activity of photocatalytic nitric oxide removal, *Nanoscale* 2019, **11**, 6360-6367.

[12] J. Liao, L. Chen, M. Sun, B. Lei, X. Zeng, Y. Sun, F. Dong, Improving visible-light-driven photocatalytic NO oxidation over BiOBr nanoplates through tunable oxygen vacancies, *J. Catal.* 2018, **39**, 779-789.

[13] G. Dong, L. Yang, F. Wang, L. Zang, C. Wang, Removal of Nitric Oxide through Visible Light Photocatalysis by g-C_3N_4 Modified with Perylene Imides, *ACS Catal*., 2016, **6**, 6511-6519.

[14] K. Li, Wen Cui, J. Li, Y. Sun, Y. Chua, Guang. Jiang, Y. Zhou, Y. Zhang, F. Dong, Tuning the reaction pathway of photocatalytic NO oxidation process to control the secondary pollution on monodisperse Au nanoparticles@ g-C_3N_4, *Chem. Eng. J.*, 2019, **378**, 122184.

[15] G. Jiang, J. Cao, M. Chen, X. Zhang, F. Dong, Photocatalytic NO oxidation on N-doped TiO_2/g-C_3N_4 heterojunction: enhanced efficiency, mechanism and reaction pathway, *Appl. Surf. Sci.*, 2018, **458**, 77-85.

[16] F. Dong, Y. Li, W. Ho, H. Zhang, M. Fu, Z. Wu, Synthesis of mesoporous polymeric carbon nitride exhibiting enhanced and durable visible light photocatalytic performance, *Chin. Sci. Bull.*, 2014, **59**, 688-698.

[17] J. Yang, X. Zhu, Z. Mo, J. Yi, J. Yan, J. Deng, Y. Xu, Y. She, J. Qian, H. Xu, H. Li, A multidimensional In_2S_3-$CuInS_2$ heterostructure for photocatalytic carbon dioxide reduction, *Inorg. Chem. Front.* 2018, **5**, 3163-3169.

[18] J. Lin, Z. Pan, X. Wang, Photochemical Reduction of CO_2 by Graphitic Carbon Nitride Polymers, *ACS Sustainable Chem. Eng.* 2014, **2**, 353-358.

[19] C. Huang, C. Chen, M. Zhang, L. Lin, X. Ye, S. Lin, M. Antonietti, X. Wang, Carbon-doped BN nanosheets for metal-free photoredox catalysis, *Nat. Commun.* 2015, **6**, 7698.

[20] Z. Mo, X. Zhu, Z. Jiang, Y. Song, D. Liu, H. Li, X. Yang, Y. She, Y. Lei, S. Yuan, H. Li, L. Song, Q. Yan, H. Xu, Porous nitrogen-rich g-C_3N_4 nanotubes for efficient photocatalytic CO_2 reduction, *Appl. Catal., B* 2019, **256**, 117854.

[21] L. Shi, T. Wang, H. Zhang, K. Chang, J. Ye, Electrostatic Self-Assembly of Nanosized Carbon Nitride Nanosheet onto a Zirconium Metal-Organic Framework for Enhanced Photocatalytic CO_2 Reduction, *Adv. Funct. Mater.* 2015, **25**, 5360-5367.

[22] S. Sato, T. Morikawa, S. Saeki, T. Kajino, T. Motohiro, Visible-Light-Induced Selective CO_2 Reduction Utilizing a Ruthenium Complex Electrocatalyst Linked to a p-Type Nitrogen-Doped Ta_2O_5 Semiconductor, *Angew. Chem. Int. Ed.* 2010, **49**, 5101-5105.

[23] R. Kuriki, M. Yamamoto, K. Higuchi, Y. Yamamoto, M. Akatsuka, D. Lu, S. Yagi, T.

Yoshida, O. Ishitani, K. Maeda, Robust Binding between Carbon Nitride Nanosheets and a Binuclear Ruthenium(II) Complex Enabling Durable, Selective CO_2 Reduction under Visible Light in Aqueous Solution, *Angew. Chem. Int. Ed.* 2017, **56**, 4867-4871.

[24] Y. Zheng, L. Lin, X. Ye, F. Guo, X. Wang, Helical graphitic carbon nitrides with photocatalytic and optical activities, *Angew. Chem. Int. Ed*. 2014, **53**, 11926-11930.

[25] P. Li, Y. Zhou, Z. Zhao, Q. Xu, X. Wang, M. Xiao, Z. Zou, Hexahedron Prism-Anchored Octahedronal CeO_2: Crystal Facet-Based Homojunction Promoting Efficient Solar Fuel Synthesis, *J. Am. Chem. Soc.* 2015, **137**, 9547-9550.

[26] B. AlOtaibi, S. Fan, D. Wang, J. Ye, Z. Mi, Wafer-Level Artificial Photosynthesis for CO_2 Reduction into CH_4 and CO Using GaN Nanowires, *ACS Catal.* 2015, **5**, 5342-5348.

[27] R. Li, J. Hu, M. Deng, H. Wang, X. Wang, Y. Hu, H. Jiang, J. Jiang, Q. Zhang, Y. Xie, Y. Xiong, Integration of an inorganic semiconductor with a metal-organic framework: a platform for enhanced gaseous photocatalytic reactions, *Adv. Mater.* 2014, **26**, 4783-4788.

[28] W. Tu, Y. Zhou, Q. Liu, S. Yan, S. Bao, X. Wang, M. Xiao, Z. Zou, An In Situ Simultaneous Reduction-Hydrolysis Technique for Fabrication of TiO_2-Graphene 2D Sandwich-Like Hybrid Nanosheets: Graphene-Promoted Selectivity of Photocatalytic-Driven Hydrogenation and Coupling of CO_2 into Methane and Ethane, *Adv. Funct. Mater.* 2013, **23**, 1743-1749.